AMERICAN JOURNAL OF BIOCHEMISTRY AND BIOTECHNOLOGY

RESEARCH ARTICLE

Fabrication of Polysaccharides from a Fermented Tea and Their Antioxidant and Hypoglycemic Viability

Jun Li[1], Lingxian Tong[2], Bing Li[2], Xuanhao Lei[1], Huili Xia[1], Feng Guan[2], Jian Ge[2]

[1]Taizhou Food and Drug Inspection and Research Institute, Taizhou, China
[2]College of Life Sciences, China Jiliang University, Hangzhou, China

*Corresponding Author: gejian16888@163.com

Abstract: The hypoglycemic effects of tea have been extensively studied, with fermented tea demonstrating notable efficacy owing to its distinct processing methods. This study involved the extraction of tea polysaccharides from Wuniuzao Black Tea (WTP) using a water extraction and ethanol precipitation method. WTP-1 and WTP-2 were obtained by separation and purification using DEAE-52 cellulose columns. Antioxidant activity was evaluated utilizing ABTS, DPPH, hydroxyl radical scavenging rates, and total reducing power assays. Hypoglycemic activity was assessed by evaluating the suppression of α-glucosidase and α-amylase integrated with experiments using Insulin resistance (IR) - HepG2 cell model. All the results proved that the WTP-1 and WTP-2 showed remarkable antioxidant activity and enzyme inhibitory effects. Following the intervention, the glucose consumption and glycogen content in IR-HepG2 cells was raised, while malondialdehyde (MDA) levels were decreased. Further, the viability of Superoxide Dismutase (SOD), Glutathione Peroxidase (GSH-Px), Hexokinase (HK), and Pyruvate Kinase (PK) were significantly enhanced. These polysaccharides also significantly altered the transcription levels of genes in the PI3K/Akt signaling pathway, causing an improvement in IR. This study provides scientific evidence that polysaccharides derived from Wuniuzao black tea alleviate IR by regulating the PI3K/Akt signaling pathway and mitigating oxidative stress, laying a groundwork for their utilization in diabetes intervention.

Keywords: Tea polysaccharides, Antioxidant Activity, Hypoglycemic Activity, Insulin Resistance (IR), PI3K/Akt Signaling Pathway

Received: 12-11-2025 | **Revised:** 14-03-2026 | **Accepted:** 15-04-2026 | **DOI:** 10.3844/ajbbsp.2026.22.02.027

Introduction

As a chronic metabolic disorder, diabetes mellitus primarily manifests as hyperglycemia and Insulin Resistance (IR) [1]. The incidence of Type 2 Diabetes Mellitus (T2DM) rises annually worldwide, primarily due to increasing rates of obesity and an aging population. In 2021, diabetes affected 10.5% of people aged 20-79 globally, a figure expected to reach 12.2% by 2045. With over 90% of cases being T2DM, this escalating condition presents a key risk to global health [2]. IR is characterized by impaired insulin action, resulting in reduced glucose uptake and utilization, subsequently leading to compensatory increases in insulin secretion by the body [3].

Oxidative stress is closely linked to various diseases, including T2DM. Insulin resistance is regarded as a crucial link between these two factors, the excessive generation of free radicals and an imbalance diminish peripheral tissue sensitivity to insulin within the antioxidant system [4], ultimately resulting in IR. Reactive oxygen species (ROS) not only damage biomolecules, including proteins, lipids, and nucleic acids, but also activate various kinases and oxidative stress signaling pathways, consequently interfering with insulin signal transduction [5]. Therefore, targeting oxidative stress to ameliorate IR is considered an effective strategy for managing T2DM. Currently, commonly used antihyperglycemic agents include acarbose, metformin, and sulfonylureas. However, these medications are often associated linked to adverse effects such as vitamin B12 deficiency, gastrointestinal discomfort (e.g., nausea and diarrhea) and hypoglycemia [6]. A rising number of researchers are focusing on the use of natural products in pharmacology to complement or replace existing treatment modalities. To date, several studies have reported that natural products derived from medicinal herbs exhibit hypoglycemic activity, including triterpenoids, flavonoids, and polyphenolic compounds [7].

Tea is an important economic crop in China among the most notable non-alcoholic beverages throughout the world, cherished for its health benefits as well as delicious and exquisite taste [8]. as important bioactive components, tea polysaccharides exhibit various functional activities, including regulating lipid metabolism [9], antioxidant effects [10], and anti-cancer abilities [11]. Tea polysaccharides possess multiple mechanisms in managing and preventing diabetes, with polysaccharides from different sources potentially exhibiting distinct mechanisms of action. For instance, acidic polysaccharides derived from Wuyi rock tea have been shown to improve plasma and hepatic lipid metabolism, significantly lowering blood sugar levels in T2DM rats [12]. Red tea polysaccharides display notable α-glucosidase inhibitory activity [13]. As noted by Zhang et al., red tea polysaccharides markedly promote the translocation of glucose transporter 2 (GLUT2) in the livers of T2DM mice via stimulating the PI3K/Akt/GLUT2 signaling pathway, thus alleviating hyperglycemia [14]. Additionally, tea polysaccharides can influence amino acids and other metabolites, regulate gut microbiota, and maintain microbial diversity, restoring the relative abundance of certain bacterial genera that decrease due to diabetes, which contributes to hypoglycemic effects in T2DM rats [15]. Therefore, tea polysaccharides may serve as effective agents in treating diabetes and its complications.

Previous studies have demonstrated that polysaccharides derived from Wuniuzao black tea exhibit significant lipid-lowering activity [16], however, their hypoglycemic effects and the underlying mechanisms remain insufficiently explored. This study demonstrated that two novel polysaccharides, designated as WTP-1 and WTP-2, were isolated and purified from Wuniuzao black tea. The antioxidant and blood sugar-lowering activities of these polysaccharides were evaluated through assessments of radical scavenging ability, total reducing power, enzyme inhibition capacity, and improvements in insulin resistance in HepG2 cells. This research aims to provide novel insights and theoretical foundations for the development of natural drugs that regulate glucose metabolism.

To demonstrate the research process and core components of this study more intuitively, the Flow Chart shown in Figure 1 is constructed. This diagram systematically presents the complete logical chain of the experimental method, clarifying the main tasks of each stage and their interrelationships.

Materials and Methods

Materials

The Wuniuzao black tea was obtained from Zhejiang Sannong Tea Co., Ltd. The α-amylase and α-glucosidase were taken from Shanghai YuanYe Biotechnology Co., Ltd. The CCK-8 kit was supplied by Beijing Soleybao Technology Co., Ltd. The assay kits for BCA, hexokinase (HK), glutathione peroxidase (GSH-Px), Glucose, Glycogen, malondialdehyde (MDA), pyruvate kinase (PK), and superoxide dismutase (SOD) were all obtained from Nanjing Jiancheng Bioengineering Institute. HepG2 cells were offered by the Institute of Cell Biology, Chinese Academy of Sciences. The DMEM low/high glucose culture medium was purchased from Gibco. (USA). The fetal bovine serum (FBS) was provided by Zhejiang Tianhang Biotechnology Co., Ltd. The TRIzol® Plus RNA Purification kit and the SuperScript™ III First-Strand Synthesis SuperMix kit were supplied by Thermo Fisher. (USA). The RNase-Free DNase Set kit was obtained from Qiagen. (Germany). We used analytical reagent grade chemicals and solvents from Sinopharm Chemical Reagent Co., Ltd. (China) for all other procedures.

DOI: 10.3844/ajbbsp.2026.22.02.027

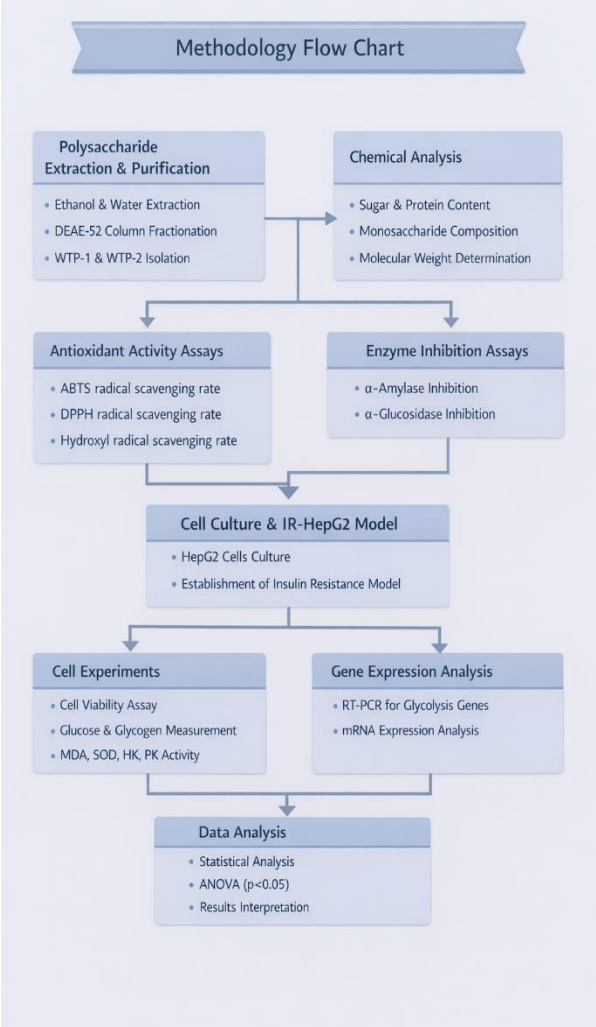

Fig. 1: Methodology Flow Chart; Wuniuzao black tea (WTP), Hexokinase (HK), pyruvate kinase (PK), malondialdehyde (MDA), superoxide dismutase (SOD), glutathione peroxidase (GSH-Px), One-way analysis of variance (ANOVA)

Extraction and Purification of Polysaccharides

The Wuniuzao black tea powder was incorporated into anhydrous ethanol at a proportion of 1:10 and heated within one water bath at 50°C while stirring for 4 h. The mixture was screened to segregate precipitate, which was subsequently dried to yield decolorized and defatted tea powder for later use. The processed tea powder was extracted with hot water at 80°C in a solid-to-liquid proportion of 1:14 (g/mL) for 3 h, followed by two additional extraction cycles. The filtrate was reduced to roughly one-quarter of its first volume using rotary evaporation. Subsequently, anhydrous ethanol was supplemented in a volume ratio of 1:4 (filtrate: ethanol), and the mixture could stand all night at 4°C for precipitation. The precipitate was gathered, and then freeze-dried to recover crude polysaccharides (WTP). The WTP solution (10 mg/mL) was loaded on a pre-equilibrated DEAE-52 cellulose column, followed by gradient elution with distilled water (DW) and NaCl solutions at concentrations of 0.1, 0.3, and 0.5 mol/L. The eluent absorbance was determined at 490 nm through the phenol-sulfuric acid method. The eluent was collected to construct an elution curve. Following concentration, the eluent was dialyzed against running water for 48 hours and then freeze-dried to yield WTP-1 and WTP-2.

Chemical Characterization

Total sugar content in the polysaccharides was determined employing the phenol-sulfuric acid method [17]. As to polysaccharides, the protein content was gauged employing the Bradford method [18]. Besides, the uronic acid content was assessed via the m-hydroxyphenyl method [19].

Monosaccharide Composition Analysis

The monosaccharide composition was analyzed employing the derivatization method with 1-Methoxy-2-Propanyl Propionate (PMP) and High-Performance Liquid Chromatography (HPLC) [20]. A total of 10 mg of polysaccharide was integrated with 5 mL of 2 mol/L trifluoroacetic acid solution, and the tube was sealed under nitrogen. The mixture was hydrolyzed for 2 h at 120°C. After that, 1 mL acid hydrolysate was supplemented to methanol and dehydrated under nitrogen. The residue was redissolved within 1 mL of 0.3 mol/L NaOH solution and mixed with PMP methanol solution, reacting at 70°C for 2 hours. Afterward, 0.3 mol/L HCl was incorporated to neutralize the solution (pH 6-7), and chloroform was added for extraction to remove PMP, repeating this step two times. Then, the aqueous phase was filtrated via a 0.45 μm microporous filter membrane to construe HPLC injection.

Chromatographic conditions: C18 column (GraceSmart RP18, 250 mm ×4.6 mm, 5 um), detection wavelength 250 nm, column temperature 30℃, flow rate 1 mL/min, injection volume 5 μL, mobile phase A was 100 mmol/L sodium phosphate buffer, mobile phase B was acetonitrile. The following elution gradient was used: 0-9 min (86% A, 14% B); 9.1-28 min (83% A, 17% B); 28.1-29 min (78% A, 22% B); 29.1-32 min (50% A, 50% B); 32.1-36 min (86% A, 14% B).

Monosaccharide Composition Analysis

The molecular weight of polysaccharides was analyzed using high-performance gel permeation chromatography (HPGPC). A 10 mg/mL solution of polysaccharide sample was fabricated and screened through one 0.45 μm microporous membrane prior to injection. Chromatograph: Agilent 1260, column: Waters Ultrahydrogel™120, 250 and 500 water-soluble gel columns (7.8×300 mm), mobile phase: 0.1 mol/L NaNO3 aqueous solution, flow rate: 1 ml/min, column temperature: 40℃, detector: G1362A (oscillometric refractive detector), injection rate: 1 ml/min. The standard curve was constructed via polyethylene glycol showing varying molecular weights. As to the polysaccharide sample solution, the molecular weight was computed via contrasting its elution time using the standard curve.

Antioxidant Activity Assay

Following the approach with corrections [21], equal volumes of 7 mmol·L^{-1} 2,2'-Azinobis-(3-ethylbenzthiazoline-6-sulphonate) (ABTS) solution and 2.5 mmol/L potassium persulfate solution were combined and reacted in darkness at room temperature (RT) for a duration of 12 to 16 hours, and diluted with DW until its absorbance value at 734 nm reached 0.70±0.05 for the ABTS working solution. 50 μL polysaccharide samples at various concentrations were incorporated into 1950 μL ABTS working solution and cultivated in the dark for 10 min at 37°C. Subsequently, the absorbance was gauged at 734 nm. The ABTS radical scavenging rate (RSA) was figured out as below (Eq. 1):

$$\text{ABTS RSA}\ (\%) = \left(1 - \frac{A_1 - A_2}{A_0}\right) \times 100\% \quad (1)$$

Where A_0 denotes the absorbance gauged via DW rather than the polysaccharide solution. A_1 denotes the absorbance gauged with polysaccharide solution. A_2 denotes the absorbance gauged via DW rather than the ABTS working solution.

Utilizing a previous method with corrections [21], equal volumes of polysaccharide sample solution and 0.2 mmol/L 2, 2-Diphenyl-1Picrylhydrazyl (DPPH) - ethanol solution were combined and mixed thoroughly. The mixture reacted in darkness for 30 min at 37°C. The absorbance was determined at 517 nm. The DPPH RSA was computed according to (Eq. 2):

$$\text{DPPH RSA}\ (\%) = \left(1 - \frac{A_1 - A_2}{A_0}\right) \times 100\% \quad (2)$$

Where A0 signifies the absorbance determined with DW instead of the polysaccharide solution. A1 represents the absorbance measured with the polysaccharide solution. A2 represents the absorbance measured with anhydrous ethanol instead of the DPPH solution.

Following the approach of Hong and colleagues [22] with corrections. 1 mL polysaccharide sample solution was combined with 1 mL of a 6 mmol/L ferrous sulfate solution and 1 mL of 10 mmol/L hydrogen peroxide solution. The mixture could react for 10 min in the dark at 37°C. Following the reaction, 1 mL of a 6 mmol/L salicylic acid solution prepared in anhydrous ethanol was supplemented, and the mixture was nurtured for 30 min in darkness at 37°C. The absorbance was gauged at 510 nm. The hydroxyl RSA was computed according to (Eq. 3):

$$\text{Hydroxyl RSA}\ (\%) = \left(1 - \frac{A_1 - A_2}{A_0}\right) \times 100\% \quad (3)$$

Where A_0 means the absorbance determined via DW rather than the polysaccharide solution. A_1 means the absorbance gauged with the polysaccharide solution. A_2 means the absorbance determined via DW rather than the salicylic acid solution.

Following the approach described by Wei et al [23] with amendments. 10 μL polysaccharide sample solution was combined with 200 μL phosphate buffer solution (pH 6.6, 0.2 mol/L) and 100 μL of 1% potassium ferricyanide solution. The mixture was cultivated for 20 min within one water bath at 50°C. After cooling, 100 μL of 10% trichloroacetic acid was added, the mixture underwent centrifugation. The supernatant (0.2 mL) was incorporated into 0.2 mL of 0.1% ferric chloride solution and 1 mL of DW. The mixture was well shaken and stood for 10 min before measuring the absorbance at 700 nm. The total reducing power was expressed as the absorbance gauged at 700 nm.

α-Glucosidase and α-Amylase Inhibition Assay

By means of a modified approach described by Cao and coworkers [24]. 40 μL polysaccharide solution was added into 40 μL α-glucosidase solution at a concentration of 0.24 U/mL. The mixture could react for 10 min at 37°C. After that, 40 μL p-nitrophenyl-β-D-glucopyranoside (pNPG) solution was employed for the reaction, which was cultured for 30 min at 37°C. The reaction ended by supplementing 500 μL of 0.2 mol/L Na2CO3 solution. The absorbance was measured at 405 nm. Acarbose served as the positive control. The inhibition rate of α-glucosidase activity was figured out as below (Eq. 4):

$$\alpha - \text{Glucosidase IA } (\%) = \left(1 - \frac{A_1 - A_2}{A_0}\right) \times 100\% \quad (4)$$

Where A_0 indicates the absorbance gauged with DW rather than polysaccharide solution; A_1 indicates the absorbance determined with polysaccharide solution; A_2 indicates the absorbance determined with DW instead of the pNPG solution.

Complying with a corrected approach of Lv and coworkers [25], 100 μL polysaccharide sample was integrated with 100 μL α-amylase solution at a concentration of 30 U/mL. The mixture could react for 10 min at 37°C. Subsequently, 100 μL of 1% soluble starch solution was supplemented. The mixture was cultured for anther 10 min at 37°C. Following this, 200 μL of 3,5-dinitrosalicylic acid solution was incorporated. The mixture was boiled for 5 min. At RT, 2 mL DW was supplemented for dilution. The absorbance was gauged at 540 nm. Acarbose served as the positive control. The inhibition rate (IA) of α-amylase activity was computed according to (Eq. 5):

$$\alpha - \text{Amylase IA } (\%) = \left(1 - \frac{A_2 - A_3}{A_0 - A_1}\right) \times 100\% \quad (5)$$

Where A_0 denotes the absorbance determined with DW rather than the polysaccharide solution; A_1 denotes the absorbance gauged with DW instead of the polysaccharide and α-amylase solutions; A_2 denotes the absorbance determined with the polysaccharide solution; A_3 denotes the absorbance gauged with DW rather than the α-amylase solution.

Cell Culture

HepG2 cells were seeded within DMEM high-glucose substrate comprising 10% FBS and 1% penicillin-streptomycin inside an incubator under 5% CO_2 at 37°C. When these cells had a density exceeding 80%, they were dissolved for passage using 0.25% trypsin. During the logarithmic growth stage, the cells were counted to plate and test.

Establishment and Validation of Insulin Resistance Cell Model (IR-HepG2)

To create the IR-HepG2 cell model, the cells were induced within serum-free low-glucose medium containing various concentrations of glucosamine (6, 12, 18, 24, 30, and 36 mM) for 24 hours. Apart from glucose consumption, cell viability was evaluated to measure the optimum induction concentration to formulate the model. The optimum concentration was selected based on the criteria of maintaining cell viability above 90% (to exclude cytotoxic effects) while achieving the lowest glucose consumption (indicating the most pronounced insulin resistance). Subsequently, cells were induced with the selected glucosamine concentrations for varying durations (12, 18, 24, 30, 36, and 48 hours). Following this, glucose consumption was gauged, with the intention of identifying the optimum induction duration. Under the identified optimal concentration and duration, glucose consumption and glycogen content were compared between the normal group (controls) and the model group to validate the successful IR-HepG2 model.

Cell Activity Test

Cells were cultivated inside one 96-well plate at a density of 1×105 cells/mL and then processed with diverse concentrations of WTP-1 and WTP-2 (50, 100, 200, 400, and 800μg/mL) for 24 hours. Cell activity was appraised via the CCK-8 assay kit per the manufacturer's recommended procedures.

Measurement of Glucose Consumption and Glycogen Content

Following the establishment of the model using the optimal method as screened earlier, IR-HepG2 cells were processed with metformin (10 mM), WTP-1 (800 μ/mL), and WTP-2 (800 μg/mL) for 24 h. Within the cell supernatant, the glucose content was determined through a glucose assay kit, while intracellular glycogen content was assessed through a glycogen assay kit. Glucose consumption (GC) was calculated according to (Eq. 6) and (Eq. 7):

$$\mathrm{GC} = G_1 - G_0 \tag{6}$$

$$\mathrm{GC\ Ratio} = \frac{GC\ \text{of Experimental Group}}{\mathrm{GC\ of\ Normal\ Group}} \tag{7}$$

Where G_1 represents the glucose content measured in the medium of each group. G_0 represents the glucose content in the blank group without cells.

Measurement of Malondialdehyde Content and Antioxidant Enzyme Activity

After cell modelling and treatment with the corresponding drugs, the intracellular MDA content, SOD and GSH-Px activity were measured following the specifications of the MDA, SOD and GSH-Px assay kit.

Measurement of HK and PK Activities

The Hexokinase (HK) and Pyruvate Kinase (PK) viability was determined complying with the guidelines of the HK and PK assay kit.

RT-PCR Detection of mRNA Expression Levels of Glycolysis-Related Genes Among HepG2 Cells

Total RNA was obtained by means of TRIzol® Plus RNA Purification and RNase-Free DNase Set kits, and its concentration and purity were assessed. cDNA was synthesized following the instructions provided in the reverse transcription kit. Quantitative PCR primers were formulated via Primer Premier 6.0 and Beacon Designer 7.8. the primers underwent synthesis by Shanghai Biological Engineering Co., Ltd. Table 1 displays the primer sequences. The reaction was conducted via the Power SYBR® Green PCR Master Mix kit, which included 0.5 μL of each upstream and downstream primer, 1 μL Power SYBR® Green Master Mix, 1.0 μL cDNA, and 8 μL sterile distilled water. The reaction conditions were listed below: The temperature was designated at 95°C for 1 min, before 40 cycles of 95°C for 15 s and 63°C for 25 s. Sample Ct values were obtained from the melting curve, with each sample analyzed in triplicate. For each gene, the relative expression levels were construed via the formula 2^ ((Ct (reference gene) - Ct (target gene))).

Table 1: RT-PCR Primers and Conditions for HepG2 Cells

Gene Name	Gene Sequence Number	Primer Sequence (5'→3')	Product Length
Human GAPDA	NM_002046.5	CCATGACAACTTTGGTATCGTGGAA GGCCATCACGCCACAGTTTC	107
Human Akt	NM_005163.2	GCCCCACTTCCCCCAGTTCT CCGCCTCTCCATCCCTCCAA	94
Human GLUT-4	M20747	TCGACCAGCATCTTCGAGACAG CCACCAACAACACCGAGACCAA	106
Human IRS-1	NM_005544	AGAACTCACTCGGCAGGCACATC TGGTGGGTAGGCAGGCATCATCT	111
Human PI3K	NM_001242466.1	GAGCGGTACAGCAAAGAATACATAGA GCCTGCTTCTTCAAGTCTTCTTCCA	155
Human G6PC1	NM_000151.4	GGCCATCACGCCACAGTTTC CCCAAGTCGAGCTGGTCTT	86
Human PEPCK	NM_004563.4	GCAGTAGGGGATGACACTGA CCCTGGGAGATGGTGACTTT	152

Data Analysis

Results were described as mean ± standard deviation. Statistical analysis was conducted through SPSS 26.0, employing one-way analysis of variance (ANOVA) aimed at assessing the significance of differences between the groups. Importantly, p-value <0.05 reached statistical significance.

Results

Chemical Composition of Polysaccharides

The yield of the WTP was 6.60%. Separated by DEAE-52 cellulose column, the elution curve is exhibited in Figure 2a. Elution with 0.3 mol/L and 0.5 mol/L NaCl solutions proved superior efficiency compared to other solutions. Consequently, these two polysaccharide fractions were collected and designated as WTP-1 and WTP-2, yielding 13.57% and 4.12%, respectively. The total sugar, uronic acid contents of the polysaccharides, protein were gauged, with standard curves presented in Figures 2(b-d). The total sugar contents of WTP, WTP-1 and WTP-2 were 46.56%, 88.13% and 79.29%, the protein content was 13.80%, 3.21%and 2.37%, and the glucuronic acid content was 40.27%, 35.43% and 26.35%, respectively.

Monosaccharide Composition and Molecular Weight of WTP-1 and WTP-2

As shown in Figure 2(h, i), the molecular weights of WTP-1 were 62488 Da (82.87%), 2239 Da (14.40%) and 618 Da (2.73%), while those of WTP-2 were 89569 Da (75.06%), 2678 Da (9.14%), and 596 Da (15.80%). The spectra of the monosaccharide composition of the monosaccharide standards, WTP-1 and WTP -2 are shown in Figure 2(e-g). The molar percentage of each monosaccharide in each sample was calculated. WTP-1 contained mainly galacturonic acid, galactose, arabinose and rhamnose showing a molar mass proportion of 44.06: 21.40: 19.73: 8.22, while the molar mass ratio of galacturonic acid, galactose, arabinose and rhamnose of WTP -2 was 31.76: 26.86: 22.85: 8.04.

Fourier Transform Infrared (FTIR) Spectroscopic Analysis of WTP-1 and WTP-2

As shown in Figure 2(j, k), The infrared spectra displayed characteristic absorptions typical of polysaccharides. Broad peaks at 3425.07 cm^{-1} and 3399.49 cm^{-1} were ascribed to the stretching and bending vibrations of O-H groups, indicating the presence of abundant hydroxyl groups in both WTP-1 and WTP-2. Absorption bands at 2923.14 cm^{-1} and 2937.74 cm^{-1} corresponded to C-H stretching vibrations, while those at 1418.10 cm^{-1} and 1417.30 cm^{-1} were assigned to C-H bending vibrations, indicating that the methyl and methylene groups were in WTP-1 and WTP-2. A weak absorption at 1740.70 cm^{-1} in the spectrum of WTP-1 was indicative of carboxyl groups, suggesting that the hyaluronic acid emerged. Both polysaccharides exhibited C = O stretching vibrations at 1619.43 cm^{-1} and 1625.54 cm^{-1}. The absorptions at 1020.30 cm^{-1} and 1099.78 cm^{-1} were assigned to the stretching vibrations of C-O-C and C-O-H, confirming that a pyranose ring structure emerged. Additionally, absorption bands in the 400-900 cm^{-1} region (437.33 cm^{-1} and 582.85 cm^{-1} for WTP-1; 640.64 cm^{-1} for WTP-2) originated from the skeletal vibrations of the pyranose ring.

WTP-1 and WTP-2 Exhibit Good Antioxidant Activity

As shown in Figure 3(a-d), the ABTS, DPPH, and hydroxyl radical scavenging performances, and the total reducing power of polysaccharides rose, as the polysaccharide concentration rose. This demonstrated a clear quantitative-effect relationship. At a concentration of 5 mg/mL, the ABTS, DPPH and hydroxyl radical scavenging capacities and the total reducing power of WTP-1 were 53%, 78%, 71% and 0.224, respectively, while those of WTP-2 were 60%, 88%, 66% and 0.934. The differences in the scavenging rates of ABTS and hydroxyl radicals between WTP-1 and WTP-2 were not significant at the same concentration. The DPPH radical scavenging capacity of WTP-2 slightly exceeded that of WTP-1 at high concentrations. The reducing ability of WTP-2 significantly surpassed that of WTP-1 at 0.01~5 mg/mL concentration.

WTP-1 and WTP-2 Significantly Suppressed the Viability of A-Glucosidase and A-Amylase

In Figure 3(e,f), the suppression effects of WTP-1 and WTP-2 upon α-glucosidase and α-amylase were significantly enhanced with the increase of their concentrations, WTP-1 displayed higher inhibitory viability against α-glucosidase at concentrations above 4 mg/mL. And the inhibition rate reached 83.22%±0.43% at 10 mg/mL. WTP-2 inhibited α-glucosidase at 8 mg/mL, and the highest inhibition rate reached 69.42%±0.51%, but slightly decreased at 10 mg/mL, which might be attributed to reduced solubility or potential interference effects at this high concentration. At low concentrations (0.5 mg/mL~2

mg/mL), the α-amylase inhibition rate of WTP-2 was significantly higher than that of WTP-1. α-Amylase inhibition of WTP-1 was greater than that of WTP-2 as the concentration rose. The α-amylase inhibitory viability of WTP -1 and WTP -2 at a concentration of 10 mg/mL reached 88.13% ± 0.36% and 75.23%±1.11%, respectively. The α-amylase inhibition of WTP -2 approached saturation at high concentrations, suggesting that WTP-1 may have stronger inhibitory potential against α-amylase at medium to high concentrations, while WTP -2 has an advantage at low concentrations. In contrast, acarbose achieved a maximum α-glucosidase inhibition rate of 98.80% ± 0.24%, with an α-amylase inhibition rate of 68.84% ± 1.49% at 0.5 mg/mL.

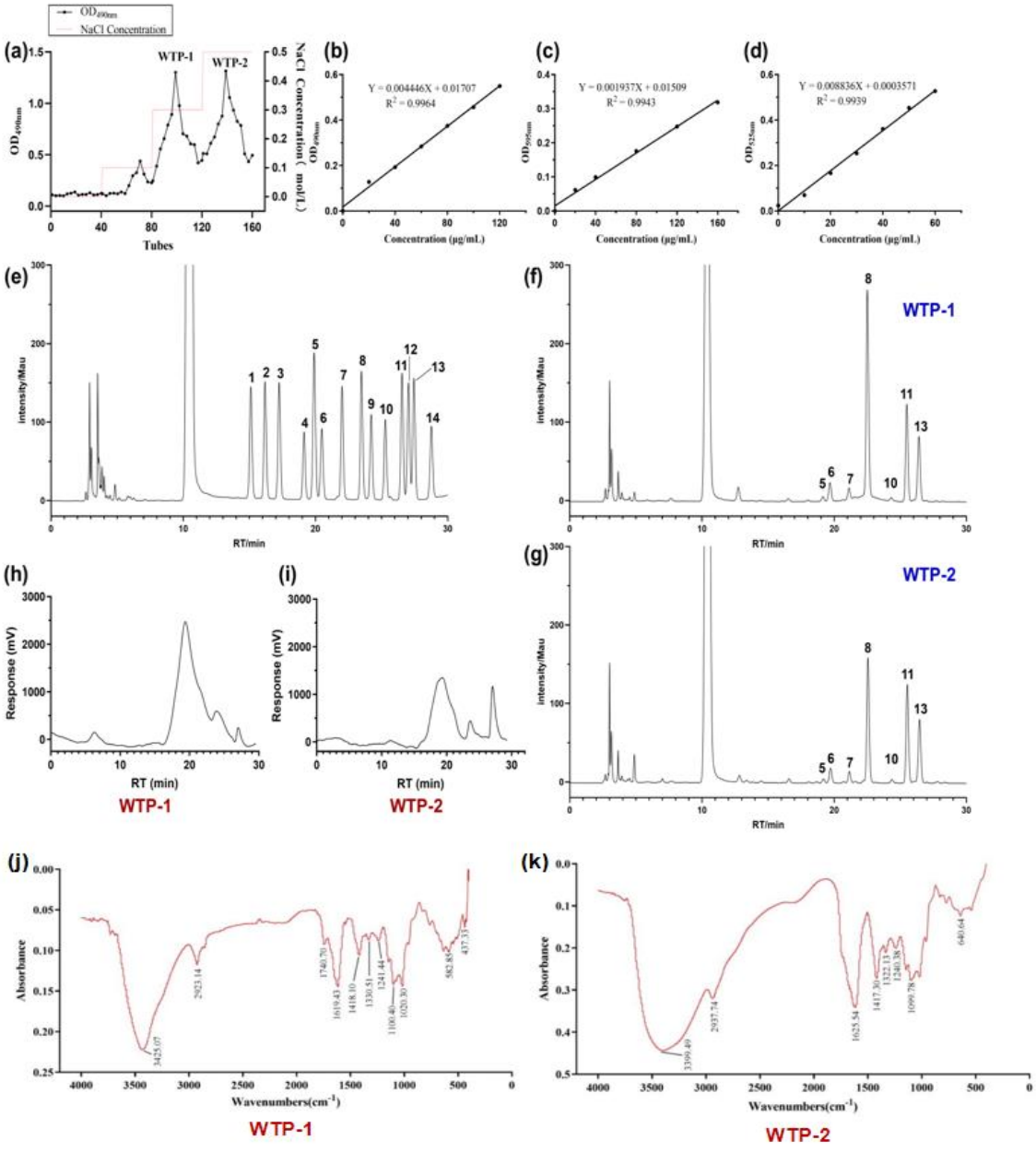

Fig. 2: Elution curve of Wuniuzao black tea (WTP) separated by DEAE-52 cellulose column (a). (OD, Optical Density) ; Standard curves for the determination of total sugar (b), protein (c) and uronic acid (d) content of polysaccharides; HPLC spectra of the monosaccharide standard (e), WTP-1 (f), and WTP-2 (g). (The numbers 1-14 in the figure correspond to arabinose, fucose, galacturonic acid, glucosamine, glucuronic acid, galactose, glucose, galacturonic acid, galactosamine, mannosonic acid, mannose, rhamnose, ribose, and xylose.); GPC spectra of the molecular weight of WTP-1 (h) and WTP-2 (i). FTIR spectra for WTP-1 (j); FTIR spectra for WTP-2 (k)

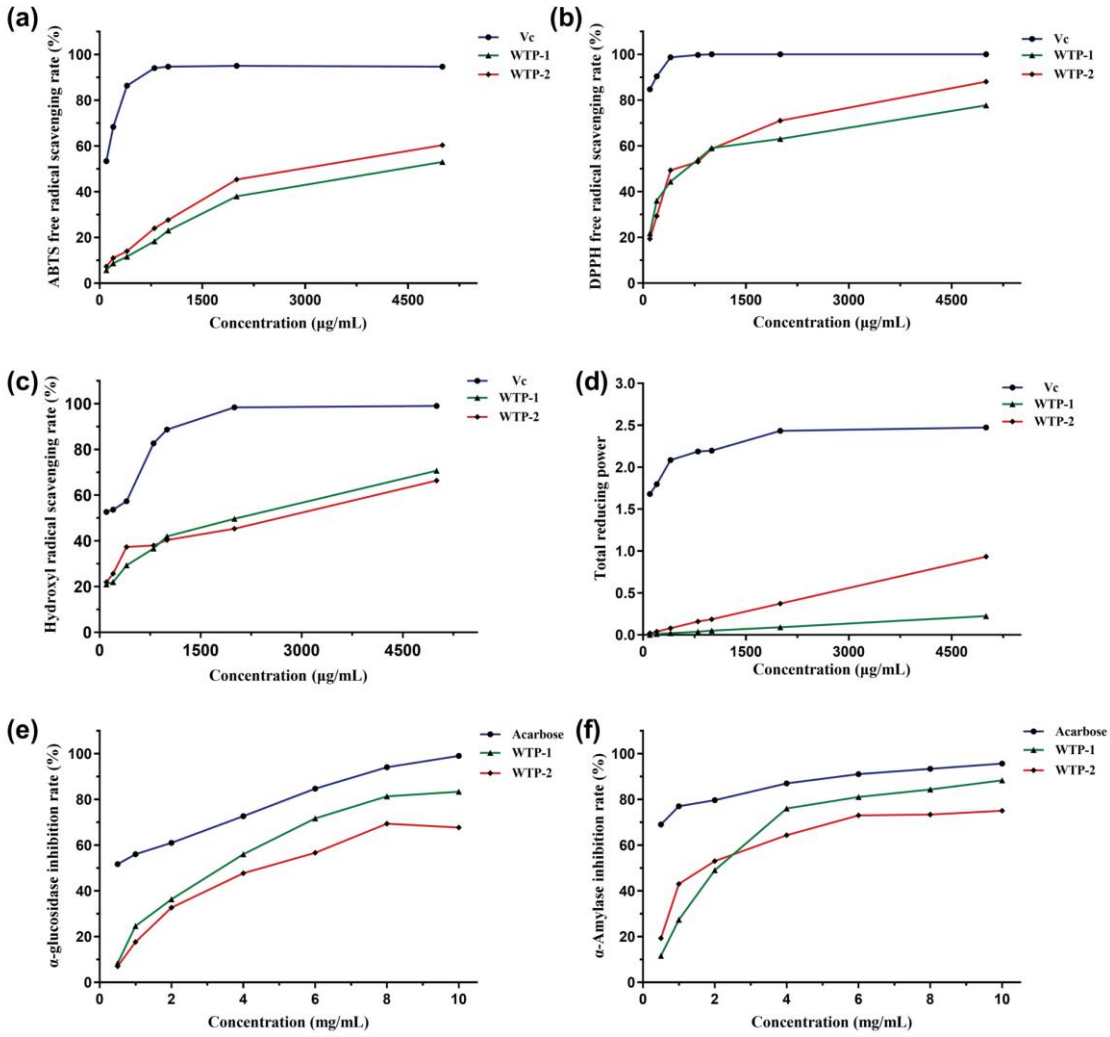

Fig. 3: Effects of WTP-1 and WTP-2 on ABTS (a), DPPH (b) and hydroxyl (c) radical scavenging rate as well as total reducing power (d). (Vitamin C (Vc) worked as the positive control.); Suppression effects of WTP-1 and WTP-2 upon α-glucosidase (e) and α-amylase (f) activity. (Acarbose served as the positive control)

Successful Establishment of IR-HepG2 Cell Model

Insulin resistance (IR) served as a key pathological characteristic of T2DM and various metabolic syndromes. It is crucial to the research on metabolism-related diseases to simulate the physiological state of dysregulation of insulin signaling pathway through the establishment of IR cell models, thus elucidating the molecular mechanisms of IR. HepG2 cells are the optimal cell line for constructing IR models. HepG2 cells were induced with varying concentrations of glucosamine (0, 6, 12, 18, 24, 30, 36 mM) for 24 hours. At a concentration of 12 mM, cell viability was above 90% (Figure 4a), and glucose consumption was the lowest (Figure 4b). Therefore, this concentration of glucosamine was chosen for establishing the cell model. HepG2 cells were further induced with 12 mM glucosamine for 12, 18, 24, 30, 36, and 48 hours. The lowest glucose consumption was observed when the induction time was 24 h (Figure 4c).

In summary, 12 mM glucosamine was selected to induce the cells for 24 h to establish an in vitro IR- HepG2 cell model for validation. In Figure 4(d,e), results indicate that compared to the normal group, the glucose consumption in the model group cells was reduced by 57.01% ($P<0.0001$), and the glycogen content was reduced by 38.94% ($P<0.0001$), suggesting that the model group cells entered into the insulin resistant state. This indicated that the IR-HepG2 cell model has been successfully established and can be used to conduct subsequent experiments.

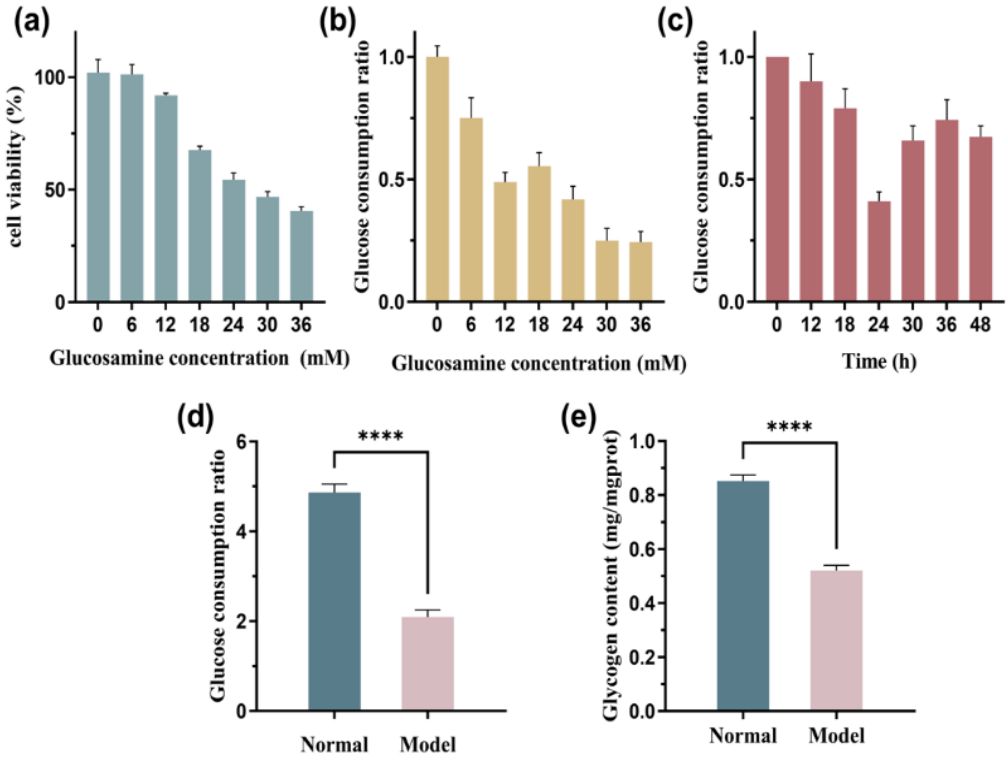

Fig. 4: Establishment and validation of the IR cell model (IR-HepG2). Impact of discrepant concentrations of glucosamine upon HepG2 cell activity(a); Impact of discrepant concentrations of glucosamine upon HepG2 cell glucose consumption(b); Effect of 12 mM glucosamine on HepG2 cell glucose consumption(c); Effects of 12 mM glucosamine induction for 24 hours upon HepG2 cell glucose consumption(d) and glycogen content(e). (n = 6). ("**" indicates P < 0.0001)**

WTP-1 and WTP-2 Significantly Promoted Glucose Consumption and Glycogen Synthesis Among IR-HepG2 Cells

Figure 5a indicates the activity of HepG2 cells processed with discrepant concentrations of WTP-1 and WTP-2 for 24 h. Obviously, within the range of 50-800μg/mL, neither WTP-1 nor WTP-2 exhibited significant cytotoxicity. Glucose consumption and liver glycogen content are important indicators of the cells' ability to uptake and utilize glucose. IR caused a reduction inside the body's sensitivity and response to insulin, thereby reducing the effectiveness of insulin-promoted glucose intake and application. Different drugs intervened IR- HepG2 cells for 24 hours. Figure 5b displays the results of cell viability. Relative to the model group, the activities of Met, WTP-1, and WTP-2 groups were remarkably increased (P<0.001). As illustrated in Figures 5(c,d), glucose consumption was decreased by 46.04% in the model group, and glycogen content was decreased by 65.69% compared to the normal group. This suggests that the model was successfully established. Relative to the model group, glucose consumption in the Met group increased by 36.81%, while WTP-1 and WTP-2 increased by 36.36% and 31.67%, respectively. The glycogen synthesis levels in each treatment group markedly differed from the model group (P < 0.001), indicating increases of 103.93%, 93.32%, and 86.02%, respectively. The effects of both polysaccharide groups were inferior to those of the positive control group, and WTP-1 was slightly more effective than WTP-2.

WTP-1 and WTP-2 Markedly Alleviated Oxidative Stress in IR-HepG2 Cells

SOD and GSH-Px function as the pivotal antioxidant enzymes within the body, responsible for eliminating ROS and peroxides. MDA, a key product of lipid peroxidation, reflects the extent of damage to biological membranes. The changes in these three markers were evaluated to assess the effects of WTP-1 and WTP-2 on oxidative stress among IR-HepG2 cells. Figures 5(e-g) exhibit the results. The MDA levels in the model group prominently increased compared to the normal group (P<0.0001), whereas the viability of SOD and GSH-Px was remarkably reduced (P<0.0001), indicating that these cells experienced oxidative stress. As opposed to the model group, MDA levels in total treatment groups were markedly decreased

(P<0.001), and SOD enzyme activity markedly raised (P<0.001). The GSH-Px enzyme viability significantly increased after treatment with Met and WTP-1 (P<0.05), while WTP-2 treatment also raised GSH-Px activity, yet the difference held statistical insignificance (P>0.05).

WTP-1 and WTP-2 Obviously Improved the Viability of Glucose Metabolic Enzymes Among Ir-HepG2 Cells

By measuring the changes in HK and PK activities among the cells, we assessed the effects of WTP-1 and WTP-2 upon glucose metabolism among IR-HepG2 cells. The results are indicated in Figures 5(h,i). Compared to the normal group, HK and PK viability in the model group cells decreased by 69.07% and 54.29%, separately. In comparison to the model group, HK and PK viability in all treatment groups showed significant increases (P<0.01). Specifically, HK and PK activities in the Met group rose by 150.76% and 93.81%, respectively; in the WTP-1 group, they increased by 114.86% and 55.08%; and in the WTP-2 group, by 63.00% and 45.71%.

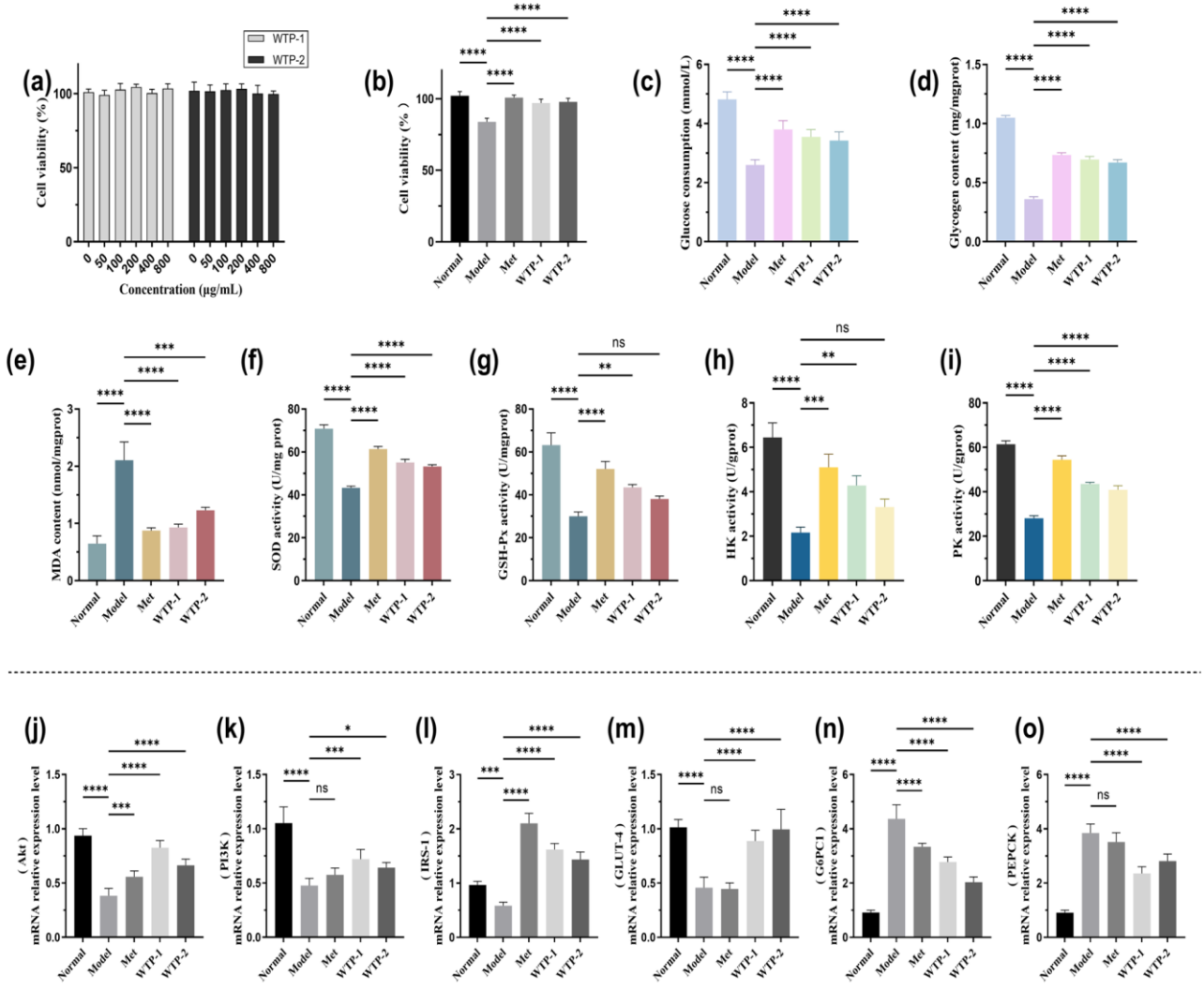

Fig. 5: Impacts of discrepant concentrations of WTP-1 and WTP-2 upon HepG2 cell activities (a); Effects of WTP-1 and WTP-2 on IR-HepG2 cell activity (b), glucose consumption (c), glycogen content (d), the contents of MDA (e), SOD (f) and GSH-PX activity (g), as well as HK (h) and PK (i) activity in IR-HepG2 cells; Impacts of WTP-1 and WTP-2 upon the expression of glucose metabolism-associated genes Akt (j), PI3K (k), IRS-1 (l), GLUT-4 (m), G6PC1 (n), and PEPCK (o) in IR-HepG2 cells. (n =6). ("ns" denotes P > 0.05, "*" denotes P < 0.05, "" denotes p < 0.01, "***" denotes P < 0.001, "****" denotes P < 0.0001)**

WTP-1 and WTP-2 Significantly Upregulated the Expressions of Akt, PI3K, IRS-1, and GLUT-4 Among IR-HepG2 Cells, While Downregulating the Expressions of G6PC1 and PEPCK

The PI3K/Akt signaling pathway is one of the key mechanisms by which insulin regulates glucose uptake and metabolism. The expressions of PI3K/Akt signaling pathway-related genes in different treatment groups were detected using RT-PCR. In Figure 5 (j-m), the expressions of Akt, PI3K, IRS-1, and GLUT-4 in the model group showed a remarkable decrease ($P<0.001$), representing only 59.07%, 54.68%, 39.48%, and 54.84% of those in the normal group, respectively. All treatment groups increased to discrepant extents in each treatment group. After the intervention of WTP-1, the expressions of Akt, PI3K, IRS-1 and GLUT-4 were markedly increased. And GLUT-4 increased to 88.08%, 68.48%, 167.41% and 87.52% of the normal group, respectively. Following WTP-2 treatment, these levels increased to 70.82%, 61.01%, 148.62% and 98.03% of the normal group, respectively. Both WTP-1 and WTP-2 significantly elevated IRS-1 expression ($p<0.0001$). phosphoenolpyruvate carboxykinase (PEPCK) and Glucose-6-phosphatase (G6Pase) are key enzymes inside the hepatic gluconeogenesis pathway. Their abnormal expressions can lead to hyperglycemia. The expressions of G6Pase catalytic subunit 1 (G6PC1) and PEPCK in the cells were assessed, as shown in Figures 5(n,o). The model group displayed a marked rise in the relative expression of G6PC1 and PEPCK ($P<0.0001$), measuring 375.32% and 323.67% of those in the normal group, respectively. Treatment with WTP-1 and WTP-2 effectively reduced these two gene expressions ($p<0.0001$).

Discussion

Wuniuzao black tea is a unique black tea produced in Yongjia County, Zhejiang Province, China. This tea is renowned for its early-picked tender buds and special processing techniques. It contains vast numbers of various bioactive compounds, like vitamins, tea polyphenols, and amino acids, offering health benefits including antioxidant properties, blood sugar reduction, and digestive enhancement. In recent years, with growing interest in health beverages, Wuniuzao black tea has gradually gained popularity in the market. However, the current development and utilization of black tea are insufficient; therefore, clarifying the mechanisms by which black tea reduces blood sugar and improves insulin resistance has important theoretical and practical implications for exploring the functions of black tea and enhancing its economic benefits.

The monosaccharide composition is fundamental to studying the primary structure of polysaccharides. Different monosaccharide compositions can lead to varying biological activities. In this study, WTP-1 and WTP-2 were isolated and purified from Wuniuzao black tea, as shown in Figure 1, with both primarily containing galacturonic acid, galactose, arabinose, and rhamnose, albeit with some differences in molar ratios. Similarly, the main components of polysaccharides extracted from Liu Bao tea by Qin and colleagues [26] were also rhamnose, galactose, and galacturonic acid. The antioxidant activity of a substance can be comprehensively assessed through four indicators: ABTS, DPPH, hydroxyl radical scavenging rate, and total reducing power. In Figure 2(a-d), we found that the radical scavenging capacity and total reducing power of WTP-1 and WTP-2 were quite similar, likely due to their analogous chemical structures. α-amylase specifically facilitates the hydrolysis of α-(1,4)-glycosidic bonds in starch, decomposing it into smaller sugars like maltose and glucose [27], and its activity directly affects the rate at which starch is converted into glucose. Likewise, α-glucosidase increases blood sugar levels by hydrolyzing glycosidic bonds to release glucose; inhibiting its activity is able to lower the level of the blood sugar [28]. As shown in Figure 2(e,f), we found that WTP-1 and WTP-2 exhibited good inhibition effects upon α-glucosidase and α-amylase at high concentrations.

Rehman et al. [29] put forward that oxidative stress was a cause of IR, damaged insulin release and glucose usage, abnormal hepatic glucose yield, and finally leads to T2DM. This study established an IR-HepG2 cell model to further assess the hypoglycemic mechanisms of WTP-1 and WTP-2. Both WTP-1 and WTP-2 were found to increase glucose consumption and intracellular glycogen content among IR-HepG2 cells. ROS can interfere with insulin signaling pathways through various mechanisms, inducing IR; conversely, metabolic disorders caused by IR (e.g., hyperglycemia) can further increase ROS production, enhancing oxidative stress. Thus, we investigated whether treatment with WTP-1 and WTP-2 could reduce oxidative damage induced by IR. As shown in Figures 4(e-g), WTP-1 and WTP-2 prominently upregulated the viability of SOD and GSH-Px while reducing MDA levels among IR-HepG2 cells, thereby improving the oxidative stress levels among these cells. HK and PK function as primary enzymes within glucose metabolism [30]. A marked decline in HK and PK activities can hinder the effective entry of glucose into the glycolytic pathway, reducing cellular glucose utilization and glycogen synthesis in the liver, ultimately impairing blood sugar regulation and exacerbating metabolic disorders [31]. Our research assessed the impacts of WTP-1 and WTP-2 on glucose metabolic function among IR-HepG2 cells via assessing changes in the viability of

HK and PK. As shown in Figure 4(h,i), WTP-1 and WTP-2 increased the viability of HK and PK, thereby influencing glycolysis and glycogen synthesis, boosting glucose absorption and usage in IR-HepG2 cells.

The insulin-mediated signaling pathway is key to lowering blood sugar and regulating overall glucose metabolism. The PI3K/Akt pathway is among the important pathways regulating insulin levels [32, 33]. When insulin ties to the insulin receptor (InsR) on cell membrane, IRS becomes phosphorylated, and the phosphorylated IRS interacts with the regulatory subunit of PI3K, activating its catalytic subunit. The subsequently generated phosphatidylinositol-3,4,5-trisphosphate (PIP3) interacts with phosphatidylinositol-dependent protein kinase 1 (PDK1) and activates Akt [34]. Activated Akt is secreted from the plasma membrane and translocates to the nucleus, cytoplasm, and mitochondria. As a serine/threonine protein kinase, Akt can phosphorylate numerous other kinases and transcription factors, thus widely modulating and engaging in protein synthesis, glycogen synthesis, lipid synthesis, cell survival, growth, and metabolic process [35]. Akt inhibits the expression of the transcription factor fork-head box O1 (FoxO1) by acting on it [36], reducing the level of key gluconeogenesis enzymes G6Pase and PEPCK [37], thereby decreasing gluconeogenesis and enhancing insulin signaling. Akt activates glycogen synthase kinase 3 (GSK3) [38], and the phosphorylation of GSK3 relieves its inhibition of glycogen synthase, resulting in increased glycogen synthesis. Glucose transporter 4 (GLUT4) is primarily found in adipose tissue and skeletal muscle [39]. Activated Akt phosphorylates AS160, promoting the translocation of GLUT4 to cell membrane and increasing cellular glucose intake [40]. As shown in Figure 4(j-o), WTP-1 and WTP-2 modulated the PI3K/Akt pathway of hepatic glucose metabolism. Compared to the normal group, the model group displayed the markedly decreased expression levels of Akt, PI3K, IRS-1, and GLUT-4. After intervention with 800 μg/mL of WTP-1 and WTP-2, the mRNA expressions of Akt, PI3K, IRS-1, and GLUT-4 among HepG2 cells were obviously upregulated. Treatment with WTP-1 and WTP-2 also effectively reduced the gene expressions of G6PC1 and PEPCK, indicating their role in attenuating gluconeogenesis by regulating G6Pase and PEPCK activity. In summary, WTP-1 and WTP-2 may regulate metabolic processes such as gluconeogenesis, glucose transport, and glycogen synthesis, via the PI3K/Akt signaling pathway in hepatic tissues, promoting glucose absorption and metabolism, ultimately improving insulin sensitivity and alleviating hepatic insulin resistance. Further investigation employing gene knockout or overexpression techniques is warranted to fully delineate the upstream and downstream regulatory mechanisms of the PI3K/Akt signaling pathway engaging in the WTP-mediated amelioration of IR.

Conclusion

To sum up, we isolated and purified two new polysaccharide components, WTP-1 and WTP-2, from Wuniuzao black tea. This study illuminated that WTP-1 and WTP-2 had good antioxidant effects and obviously inhibited α-glucosidase and α-amylase, ameliorating IR in IR-HepG2 cells, suggesting that these polysaccharides could serve as functional food constituents for the adjunctive therapy of diabetes.

Acknowledgment

We wish to show our gratitude to the National Natural Science Foundation of China (31100499 and 31672394) and the Key Project of Science and Technology Plan of Zhejiang Provincial Market Supervision and Administration Bureau (ZD2025026).

Funding Information

This research received financial supports from the National Natural Science Foundation of China (31100499 and 31672394) and the Key Project of Science and Technology Plan of Zhejiang Provincial Market Supervision and Administration Bureau (ZD2025026).

Author's Contributions

Jun Li: Designed the research plan and experiments.
Lingxian Tong: Contributed to the writing of the manuscript.
Bing Li, Xuanhao Lei and Huili Xia: Conducted partial experimental procedures.

Feng Guan: Designed and guided the experiments.
Jian Ge: Analyzed the data and reviewed the manuscript.

References

1. Roden, M., & Shulman, G. I. (2019). The integrative biology of type 2 diabetes. Nature. https://doi.org/10.1038/s41586-019-1797-8
2. Sun, H., Saeedi, P., Karuranga, S., Pinkepank, M., Ogurtsova, K., Duncan, B. B., Stein, C., Basit, A., Chan, J. C. N., Mbanya, J. C., Pavkov, M. E., Ramachandaran, A., Wild, S. H., James, S., Herman, W. H., Zhang, P., Bommer, C., Kuo, S., Boyko, E. J., & Magliano, D. J. (2022). IDF Diabetes Atlas: Global, regional and country-level diabetes prevalence estimates for 2021 and projections for 2045. Diabetes Research and Clinical Practice, 183, 109119. https://doi.org/10.1016/j.diabres.2021.109119
3. Petersen, M. C., & Shulman, G. I. (2018). Mechanisms of Insulin Action and Insulin Resistance. Physiological Reviews, 98(4), 2133-2223. https://doi.org/10.1152/physrev.00063.2017
4. Newsholme, P., Cruzat, V. F., Keane, K. N., Carlessi, R., & de Bittencourt, P. I. H. (2016). Molecular mechanisms of ROS production and oxidative stress in diabetes. Biochemical Journal, 473(24), 4527-4550. https://doi.org/10.1042/bcj20160503c
5. Ahmad, W., Ijaz, B., Shabbiri, K., Ahmed, F., & Rehman, S. (2017). Oxidative toxicity in diabetes and Alzheimer's disease: mechanisms behind ROS/ RNS generation. Journal of Biomedical Science, 24(1), 76. https://doi.org/10.1186/s12929-017-0379-z
6. Vestergaard, P. (2021). Diabetes and its Complications - Contemporary Treatment and Potential Side Effects of Drugs to Treat Diabetes. Current Drug Safety, 16(1), 1-1. https://doi.org/10.2174/1574886316012102030936l5
7. El-Nashar, H. A. S., Mostafa, N. M., El-Shazly, M., & Eldahshan, O. A. (2021). The Role of Plant-Derived Compounds in Managing Diabetes Mellitus: A Review of Literature from 2014 To 2019. Current Medicinal Chemistry, 28(23), 4694-4730. https://doi.org/10.2174/0929867328999201123194510
8. Hu, T., Wu, P., Zhan, J., Wang, W., Shen, J., Wang, M., Ho, C.-T., & Li, S. (2022). Structure variety and its potential effects on biological activity of tea polysaccharides. Food Science and Human Wellness, 11(3), 587-597. https://doi.org/10.1016/j.fshw.2021.12.015
9. Wang, Y., Li, T., Liu, Y., Yang, C., Liu, L., Zhang, X., & Yang, X. (2022). Heimao tea polysaccharides ameliorate obesity by enhancing gut microbiota-dependent adipocytes thermogenesis in mice fed with high fat diet. Food & Function, 13(24), 13014-13027. https://doi.org/10.1039/d2fo02415b
10. Xiao, K., Shi, Y., Liu, S., Chen, Y., Ni, D., & Yu, Z. (2023). Compositions and Antioxidant Activity of Tea Polysaccharides Extracted from Different Tea (Camellia sinensis L.) Varieties. Foods, 12(19), 3584. https://doi.org/10.3390/foods12193584
11. Zhou, Y., Zhou, X., Hong, T., Qi, W., Zhang, K., Geng, F., & Nie, S. (2021). Lysosome-mediated mitochondrial apoptosis induced by tea polysaccharides promotes colon cancer cell death. Food & Function, 12(21), 10524-10537. https://doi.org/10.1039/d1fo00987g
12. Wu, Z., Zeng, W., Zhang, X., & Yang, J. (2022). Characterization of Acidic Tea Polysaccharides from Yellow Leaves of Wuyi Rock Tea and Their Hypoglycemic Activity via Intestinal Flora Regulation in Rats. Foods, 11(4), 617. https://doi.org/10.3390/foods11040617
13. Xiang, G., Sun, H., Chen, Y., Guo, H., Liu, Y., Li, Y., Lu, C., & Wang, X. (2023). Antioxidant and hypoglycemic activity of tea polysaccharides with different degrees of fermentation. International Journal of Biological Macromolecules, 228, 224-233. https://doi.org/10.1016/j.ijbiomac.2022.12.114
14. Zhang, Z., Deng, X., Chen, R., Li, Q., Sun, L., Cao, J., Lai, Z., Lai, X., Wang, Z., Sun, S., & Zhang, L. (2024). Effect of Black Tea Polysaccharides on Alleviating Type 2 Diabetes Mellitus by Regulating PI3K/Akt/GLUT2 Pathway. Foods, 13(12), 1908. https://doi.org/10.3390/foods13121908
15. Li, H., Fang, Q., Nie, Q., Hu, J., Yang, C., Huang, T., Li, H., & Nie, S. (2020). Hypoglycemic and Hypolipidemic Mechanism of Tea Polysaccharides on Type 2 Diabetic Rats via Gut Microbiota and Metabolism Alteration. Journal of Agricultural and Food Chemistry, 68(37), 10015-10028. https://doi.org/10.1021/acs.jafc.0c01968
16. Zou, X., Dong, Z., Liu, W., Zhao, J., Guan, F., & Ge, J. (2024). Modulation Mechanism of Wuniuzao Dark Tea Polysaccharide on Lipid Metabolism in Hyperlipidemic Mice Induced by High-Fat Diet. Plant Foods for Human Nutrition, 79(1), 173-181. https://doi.org/10.1007/s11130-024-01145-2
17. Chen, J., Li, L., Zhang, X., Wan, L., Zheng, Q., Xu, D., Li, Y., Liang, Y., Chen, M., Li, B., & Chen, Z. (2021). Structural characterization of polysaccharide from Centipeda minima and its hypoglycemic activity through alleviating insulin resistance of hepatic HepG2 cells. Journal of Functional Foods, 82, 104478. https://doi.org/10.1016/j.jff.2021.104478
18. Bradford, M. M. (1976). A rapid and sensitive method for the quantitation of microgram quantities of protein utilizing the principle of protein-dye binding. Analytical Biochemistry, 72(1-2), 248-254. https://doi.org/10.1016/0003-2697(76)90527-3
19. Filisetti-Cozzi, T. M. C. C., & Carpita, N. C. (1991). Measurement of uronic acids without interference from neutral sugars. Analytical Biochemistry, 197(1), 157-162. https://doi.org/10.1016/0003-2697(91)90372-z
20. Kim, H., Kwak, B.-S., Hong, H.-D., Suh, H.-J., & Shin, K.-S. (2016). Structural features of immunostimulatory polysaccharide purified from pectinase hydrolysate of barley leaf. International Journal of Biological Macromolecules, 87, 308-316. https://doi.org/10.1016/j.ijbiomac.2016.02.072
21. Guo, R., Zhang, J., Liu, X., Li, X., Sun, X., Kou, Y., Li, D., Liu, Y., Zhang, H., & Wu, Y. (2022). Pectic polysaccharides from Biluochun Tea: A comparative study in macromolecular characteristics, fine structures and radical scavenging activities in vitro. International Journal of Biological Macromolecules, 195, 598-608. https://doi.org/10.1016/j.ijbiomac.2021.12.004
22. Hong, Q., Chen, G., Wang, Z., Chen, X., & Kan, J. (2023). Effects of different thermal processing methods on bioactive components, phenolic compounds, and antioxidant activities of Qingke (highland hull-less barley). Food Science and Human Wellness, 12(1), 119-129. https://doi.org/10.1016/j.fshw.2022.07.030

23. Wei, Q., & Zhang, Y. (2023). Ultrasound-assisted polysaccharide extraction from Cercis chinensis and properites, antioxidant activity of polysaccharide. Ultrasonics Sonochemistry, 96, 106422. https://doi.org/10.1016/j.ultsonch.2023.106422
24. Cao, C., Huang, Q., Zhang, B., Li, C., & Fu, X. (2018). Physicochemical characterization and in vitro hypoglycemic activities of polysaccharides from Sargassum pallidum by microwave-assisted aqueous two-phase extraction. International Journal of Biological Macromolecules, 109, 357-368. https://doi.org/10.1016/j.ijbiomac.2017.12.096
25. Lv, Q.-Q., Cao, J.-J., Liu, R., & Chen, H.-Q. (2021). Structural characterization, α-amylase and α-glucosidase inhibitory activities of polysaccharides from wheat bran. Food Chemistry, 341, 128218. https://doi.org/10.1016/j.foodchem.2020.128218
26. Qin, H., Huang, L., Teng, J., Wei, B., Xia, N., & Ye, Y. (2021). Purification, characterization, and bioactivity of Liupao tea polysaccharides before and after fermentation. Food Chemistry, 353, 129419. https://doi.org/10.1016/j.foodchem.2021.129419
27. Zhang, N., & Yang, G. (2023). α-amylase detection methods and applications. National Library of Medicine, 39(3), 898-911.
28. Kumar, V., Prakash, O., Kumar, S., & Narwal, S. (2011). α-glucosidase inhibitors from plants: A natural approach to treat diabetes. Pharmacognosy Reviews, 5(9), 19. https://doi.org/10.4103/0973-7847.79096
29. Rehman, K., & Akash, M. S. H. (2017). Mechanism of Generation of Oxidative Stress and Pathophysiology of Type 2 Diabetes Mellitus: How Are They Interlinked? Journal of Cellular Biochemistry, 118(11), 3577-3585. https://doi.org/10.1002/jcb.26097
30. Jansen, G., Koenderman, L., Rijksen, G., Cats, B. P., & Staal, G. E. J. (1985). Characteristics of hexokinase, pyruvate kinase, and glucose-6-phosphate dehydrogenase during adult and neonatal reticulocyte maturation. American Journal of Hematology, 20(3), 203-215. https://doi.org/10.1002/ajh.2830200302
31. Wang, D., Zhao, X., & Liu, Y. (2017). Hypoglycemic and hypolipidemic effects of a polysaccharide from flower buds of Lonicera japonica in streptozotocin-induced diabetic rats. International Journal of Biological Macromolecules, 102, 396-404. https://doi.org/10.1016/j.ijbiomac.2017.04.056
32. Deng, T., Zhang, Y., Wu, Y., Ma, P., Duan, J., Qin, W., Yang, X., & Chen, M. (2018). Dibutyl phthalate exposure aggravates type 2 diabetes by disrupting the insulin-mediated PI3K/AKT signaling pathway. Toxicology Letters, 290, 1-9. https://doi.org/10.1016/j.toxlet.2018.03.004
33. Kubota, H., Noguchi, R., Toyoshima, Y., Ozaki, Y., Uda, S., Watanabe, K., Ogawa, W., & Kuroda, S. (2012). Temporal Coding of Insulin Action through Multiplexing of the AKT Pathway. Molecular Cell, 46(6), 820-832. https://doi.org/10.1016/j.molcel.2012.04.018
34. Manning, B. D., & Toker, A. (2017). AKT/PKB Signaling: Navigating the Network. Cell, 169(3), 381-405. https://doi.org/10.1016/j.cell.2017.04.001
35. Saltiel, A. R. (2021). Insulin signaling in health and disease. Journal of Clinical Investigation, 131(1), e142241. https://doi.org/10.1172/JCI142241
36. Xing, Y., Li, A., Yang, Y., Li, X., Zhang, L., & Guo, H. (2018). The regulation of FOXO1 and its role in disease progression. Life Sciences, 193, 124-131. https://doi.org/10.1016/j.lfs.2017.11.030
37. He, L., Li, Y., Zeng, N., & Stiles, B. L. (2020). Regulation of basal expression of hepatic PEPCK and G6Pase by AKT2. Biochemical Journal, 477(5), 1021-1031. https://doi.org/10.1042/bcj20190570
38. Zhao, M., Lu, M., Zeng, Y., He, S., Feng, Y., Yang, S., & Jang, W. (2023). Taraxasterol Inhibits Hepatic Gluconeogenesis and Increases Glycogen Synthesis via the PI3K/Akt Signaling Pathway. Natural Product Communications, 18(3), 1934578X231154068. https://doi.org/10.1177/1934578x231154068
39. Govers, R. (2014). Cellular Regulation of Glucose Uptake by Glucose Transporter GLUT4. Advances in Clinical Chemistry, 66, 173-66. https://doi.org/10.1016/b978-0-12-801401-1.00006-2
40. Sharma, M., & Dey, C. S. (2021). AKT ISOFORMS-AS160-GLUT4: The defining axis of insulin resistance. Reviews in Endocrine and Metabolic Disorders, 22(4), 973-986. https://doi.org/10.1007/s11154-021-09652-2